Toward magnonic logic and neuromorphic computing : controlling spin waves by spin-polarized current

Towards Magnonic Logic and Neuromorphic Computing: Controlling Spin-Waves by Spin-Polarized Current

Raí M. Menezes,[1,2] Jeroen Mulkers,[3] Clécio C. de Souza Silva,[1] Bartel Van Waeyenberge,[3] and Milorad V. Milošević[2,*]

[1] *Departamento de Física, Universidade Federal de Pernambuco,*
Cidade Universitária, 50670-901, Recife-PE, Brazil
[2] *NANOlab Center of Excellence & Department of Physics,*
University of Antwerp, Groenenborgerlaan 171, B-2020 Antwerp, Belgium
[3] *DyNaMat Lab, Department of Solid State Sciences, Ghent University, Ghent, Belgium*

Spin-waves (magnons) are among the prime candidates for building fast yet energy-efficient platforms for information transport and computing. We here demonstrate theoretically and in state-of-the-art micromagnetic simulation the effects that strategically-injected spin-polarized current can have on controlling magnonic transport. We reveal analytically that the Zhang-Li spin-transfer-torque induced by applied current is analogous to the Dzyaloshinskii-Moriya interaction for scattering the magnons in the linear regime, to then provide a generalized Snell's law that describes the spin-wave propagation across regions with different current densities. We validate the latter in numerical simulations of realistic systems, and exemplify how these findings may help advance the design of spin-wave logic and neuromorphic computing devices.

I. INTRODUCTION

The development of neuromorphic computing hardware has attracted significant attention in recent years as such platforms are capable of performing complex information processing tasks, such as classification and pattern recognition of various types of data, from e-commerce to scientific content[1–3]. A central challenge of this research is the requirement of highly interconnected systems, inspired by the biological concepts of the human brain. Interestingly, wave-based physical systems have been demonstrated to operate as recurrent neural networks[4–6], where interference patterns in the propagating substrate can realize an all-to-all interconnection between points of the substrate that mimic the action of artificial neurons by scattering and recombining input waves in order to extract their information.

Similar to other wave phenomena in physics, spin-waves (magnons) travel through space accompanied by a transfer of energy, which if precisely controlled can lead to fast information transport and computing applications in the nanometric to micrometric scale[7,8]. Spin-waves are readily demonstrated as a promising platform for performing logic operations[9,10] and the recent theoretical advances in wave-based computation can pave the way for spintronic hardware in the field of artificial intelligence[11]. However, even though extensive research has been carried out in recent years, the precise manipulation of spin waves in nanostructures has not been entirely mastered and needs to be advanced for the benefit of functional magnonic devices.

One manner of manipulating the spin textures in magnetic materials is by the application of spin-polarized (SP) currents, having (part of the) spins of the moving electrons aligned. The interaction of a SP current with the localized magnetic moments results in a torque on the magnetization, dubbed a Zhang-Li spin-transfer-
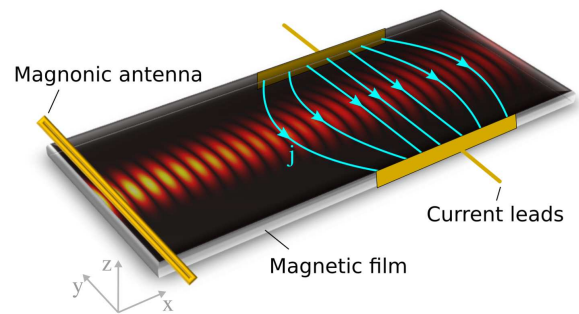
FIG. 1. **Schematic illustration of a SW facing a non-uniform distribution of the SP current**. The SW (in red) is induced by the input antenna on the left side and propagates along the magnetic film. Voltage electrodes induce the distributed spin current density (j) which can be tuned to control the SW propagation.

torque (STT)[12]. Being able to affect the orientation of the magnetization, STT has become nearly unavoidable in the design of spintronic nanodevices[13]. The effect and applicability of the STT was demonstrated in racetrack memory concepts, where the position of local magnetic structures, such as domain walls and skyrmions, is controlled by in-plane currents[14,15]. Moreover, not only do spin currents modify the equilibrium magnetic state, they can also significantly influence the propagation of spin waves (SWs). For instance, in Ref. 16 the authors derived the dispersion relation of SWs in a ferromagnet subjected to a uniform spin current. The applied current introduces a term proportional to the wavevector k in the spin-wave dispersion relation. The nonreciprocity in the dispersion relation for waves with a k vector in the same or the opposite direction as the current flow causes Doppler shift[17], as first validated experimentally by Vlaminck and Bailleul[18].

A similar nonreciprocal term in the dispersion rela-

tion can also be induced by an electric field[19] or by the antisymmetric exchange interaction, also known as Dzyaloshinskii-Moriya interaction (DMI)[20]. Analogously to the Doppler shift induced by the currents, a frequency shift has been measured in ferromagnetic materials possessing DMI[21]. For heterochiral ferromagnets (*i.e.*, with spatially varying DMI), the reciprocal term causes a nontrivial refraction of spin waves at interfaces between regions with different DMI, as described by a generalized Snell's law in Ref. 22. In this regard, the equivalency in the dispersion relations of SWs in the presence of DMI and spin current suggests that a spatially varying current density (as illustrated in Fig. 1) can be used to manipulate the propagation of SWs. In this work, we detail the effect of a SP current on controlling the propagation of spin-waves. We show that the Zhang-Li STT induced by in-plane current has analogous effect to DMI for confining and controlling the propagation direction of magnons in the linear regime. We proceed to derive a Snell's law to describe the scattering of spin-waves between regions with different current densities, and validate it by advanced simulations including solving Poisson's equation within the micromagnetic framework. Finally, we present selected tailored examples to illustrate how strategically applied current can be employed to advance logic and neuromorphic computing devices based on spin-waves.

The paper is organized as follows. In Sec. II, we present the micromagnetic model for ferromagnetic films subjected to an applied spin-polarized current. We then introduce the Poisson solver employed for accurately calculating the interaction of SWs with nonuniform current distributions and delineate the SW dispersion relation under SP current, detailing the effect of the spin current on controlling the propagation direction of SWs. In Sec. III we analytically demonstrate the generalized Snell's law that describes the SW propagation across regions with different current densities and validate it by numerical simulations that involve solving Poisson's equation within the micromagnetic framework. Section IV showcases potential applications, exemplified by the numerical reproduction of a multichannel SW selector and an artificial neural network hardware designed for proof-of-concept classification tasks. Our results are summarized in Sec. V.

II. THEORETICAL FRAMEWORK AND FUNDAMENTALS OF SPIN-WAVE PROPAGATION UNDER APPLIED CURRENT

A. Micromagnetic model

Within the micromagnetic framework, we describe the magnetization of a thin extended ferromagnetic film by considering the vector field $\vec{M}(\mathbf{r}) = M_s \vec{m}(\mathbf{r})$ with constant magnetization modulus $|\vec{M}| = M_s$ and the normalized magnetization direction $\vec{m}(\mathbf{r})$ at each point $\mathbf{r} \in \mathbb{R}^2$

of the film[23]. The dynamics of the magnetization is governed by the Landau-Lifshitz-Gilbert (LLG) equation

$$\dot{\vec{m}} = -\gamma \vec{m} \times \vec{H}_{\text{eff}} + \alpha \vec{m} \times \dot{\vec{m}} + \vec{\tau}_{\text{STT}}, \qquad (1)$$

where γ is the gyromagnetic ratio, α the dimensionless damping factor, and $\vec{H}_{\text{eff}}$ the effective field, which can be derived from the free energy $E[\vec{m}]$ by taking the functional derivative with respect to the magnetization: $\vec{H}_{\text{eff}} = -\delta E/\delta \vec{M}$.

We extend the LLG equation by adding the torque $\vec{\tau}_{\text{STT}}$ which includes the adiabatic and non-adiabatic STT terms derived by Zhang and Li[12]:

$$\vec{\tau}_{\text{STT}} = \vec{m} \times (\vec{m} \times (\mathbf{u} \cdot \nabla)\vec{m}) + \beta \vec{m} \times (\mathbf{u} \cdot \nabla)\vec{m}, \quad (2)$$

where

$$\mathbf{u} = -\frac{\mu_B P}{e M_s (1 + \beta^2)} \mathbf{j}. \qquad (3)$$

Here, ∇ is the two-dimensional differential operator, β is a dimensionless constant that represents the degree of non-adiabaticity, e the elementary charge and μ_B the Bohr magneton. The polarization P is a property of the ferromagnet and does not depend on the magnetization. Although $\mathbf{u}$ has the units of velocity, we refer to it as *current* since it is proportional to the SP current density $\mathbf{j}$. Note that the most prominent effect of the STT is best understood by assuming small dissipation terms ($\alpha \approx 0$ and $\beta \approx 0$). In that case it is easy to prove that the solution of the LLG equation is given by $\vec{m}(\mathbf{r} - \mathbf{u}t; t)$ if $\vec{m}(\mathbf{r}; t)$ is the solution in absence of the STT. Put differently, adding the STT shifts the solution with a velocity $\mathbf{u}$[24]. For instance, due to the STT, relaxed local structures such as domain walls and skyrmions will move with a velocity $\mathbf{v} = \mathbf{u}$ when the current is switched on. Accordingly, a SW packet traveling in the film will gain an additional velocity equal to $\mathbf{u}$. This insight will help the intuitive understanding of the results further presented in this paper, where we detail the effect of a non-uniform static current $\mathbf{u}(\mathbf{r})$ on the propagation of SWs.

The dynamics of the magnetization depends strongly on the characteristics of the magnetic film, incorporated in the free energy functional. In this paper, we take into account the contribution of exchange interaction and Zeeman energy due to applied bias magnetic field:

$$E[\vec{m}] = \iint \left[A(\nabla \vec{m})^2 - \vec{H} \cdot \vec{m} \right] \mathrm{d}x \mathrm{d}y, \qquad (4)$$

with exchange stiffness $A > 0$ and bias field $\vec{H}$. In our calculations, we consider SWs in the exchange regime and therefore neglect dipolar interactions. The effect of such interactions on our results will be discussed in Sec. IV B for a specific case.

B. Current distribution

To simulate the SW system in the presence of the spin current, we employ the micromagnetic simulation pack-

age Mumax3[25,26] on a thin ferromagnetic film. To precisely calculate the interaction of SWs with the nonuniform current distributions, we implemented a Poisson solver in the micromagnetic simulations, where a custom module has been added to the simulation package Mumax3. Considering a set of contact, micromagnetic cells where an applied voltage U is fixed, the generalized Poisson equation $\nabla \cdot (\sigma[\vec{m}] \cdot \nabla \Phi) = 0$ is solved using a conjugate gradient method, for the considered geometries, from where the current density $\mathbf{j} = -\sigma[\vec{m}] \cdot \nabla \Phi$ is calculated. The electric potential Φ satisfies the Poisson equation with the boundary conditions $\Phi|_{\text{contact}} = U$. Moreover, since the relaxation of the current paths occurs on a short time scale compared to the dynamics of the magnetization, $\mathbf{j}$ can be calculated self-consistently based on the anisotropic magnetoresistance (AMR) effect, where the conductivity tensor $\sigma[\vec{m}]$ depends on the magnetization and it is written as[27]

$$\sigma[\vec{m}] = \sigma_0 \left[\mathbb{1} - \frac{6a}{6+a} \begin{pmatrix} m_x^2 - \frac{1}{3} & m_x m_y & m_x m_z \\ m_y m_x & m_y^2 - \frac{1}{3} & m_y m_z \\ m_z m_x & m_z m_y & m_z^2 - \frac{1}{3} \end{pmatrix} \right],$$

(5)

where σ_0 is the material conductivity and a the AMR ratio.

C. Spin-wave dispersion under applied current

To calculate the SW dispersion under applied current, we consider a ferromagnetic (field-polarized) ground state magnetization in which the magnetization is aligned with the bias field $\vec{H}$. To study small deviations from the ground state it is useful to construct the right-handed coordinate system $(\hat{e}_a, \hat{e}_b, \hat{e}_0)$ with $\hat{e}_0 \parallel \vec{H}$. The effective field in this coordinate system becomes

$$\vec{H}_{\text{eff}}(\mathbf{r}, t) = \begin{bmatrix} \frac{2A}{M_s} \nabla^2 m_a(\mathbf{r}, t) \\ \frac{2A}{M_s} \nabla^2 m_b(\mathbf{r}, t) \\ \frac{2A}{M_s} \nabla^2 m_0(\mathbf{r}, t) + H_0 \end{bmatrix},$$

(6)

where $\vec{m} = (m_a, m_b, m_0)$ and $H = (0, 0, H_0)$. Here and in the next section, we focus on first order deviations from the ground state and consider the SW solution as $m_0 \approx 1$, $m_a = A_0 e^{i(\mathbf{k} \cdot \mathbf{r} - \omega t) - \mu t}$ and $m_b = i A_0 e^{i(\mathbf{k} \cdot \mathbf{r} - \omega t) - \mu t}$, where $A_0 \ll 1$ represents the SW amplitude; ω is the SW angular frequency; $\mathbf{k}$ is the wave vector, and μ represents the damping of the SW. Substituting that into the LLG equation [Eq. (1)], with STT term given by Eq. (2) and effective field from Eq. (6), yields the dispersion relation (see supplementary material[28])

$$\omega = \frac{\gamma H_0}{1 + \alpha^2} \left(1 + \xi^2 k^2 \right) + \frac{1 + \alpha\beta}{1 + \alpha^2} \mathbf{u} \cdot \mathbf{k},$$

(7)

and damping parameter

$$\mu = \alpha\omega - \beta \mathbf{u} \cdot \mathbf{k},$$

(8)

where we define the length scale $\xi = \sqrt{2A/H_0 M_s}$. Note that the damping μ of the SW decreases if the wave vector $\mathbf{k}$ is parallel to the electron flow $\mathbf{u}$. Consequently, the attenuation length of a spin wave can be increased by applying a current opposite to the propagation direction, as predicted earlier by Seo et al.[29].

1. Propagation direction

The dispersion relation consists out of circular isofrequencies in k-space, which are shifted away from the origin due to the current. The center of the circular isofrequency is given by

$$\mathbf{k}_0 = -\frac{1 + \alpha\beta}{2\gamma H_0 \xi^2} \mathbf{u},$$

(9)

and the radius by

$$k_g = |\mathbf{k} - \mathbf{k}_0| = \sqrt{\frac{1 + \alpha^2}{\gamma H_0 \xi^2} (\omega - \omega_0)},$$

(10)

with the minimal frequency $\omega_0 = \gamma H_0 (1 - \xi^2 k_0^2)$.

The propagation velocity $\mathbf{v}$ of a wave packet is given by the gradient of the frequency in k-space:

$$\mathbf{v} = \nabla_k \omega = \frac{2\gamma H_0 \xi^2}{1 + \alpha^2} \mathbf{k} + \frac{1 + \alpha\beta}{1 + \alpha^2} \mathbf{u} = \frac{2\gamma H_0 \xi^2}{1 + \alpha^2} (\mathbf{k} - \mathbf{k}_0),$$

(11)

where $\mathbf{k}_g = \mathbf{k} - \mathbf{k}_0$ defines the propagation direction. The velocity of the wave packet can be separated as

$$v_\parallel = \frac{\gamma H_0 \xi^2}{1 + \alpha^2} 2k + \frac{1 + \alpha\beta}{1 + \alpha^2} u_\parallel, \quad v_\perp = \frac{1 + \alpha\beta}{1 + \alpha^2} u_\perp, \quad (12)$$

where $\parallel$ and $\perp$ denote the component parallel and perpendicular to the wave vector respectively. Notice that, in general, the propagation direction is not parallel to the wave vector $\mathbf{k}$, and the SW can be deflected in the presence of applied current.

III. GENERALIZED SNELL'S LAW FOR SPIN WAVES IN PRESENCE OF NONUNIFORM CURRENT DISTRIBUTION

Let us now examine the propagation of SWs when experiencing nonuniform current distributions. For simplicity, we start with the example of a SW propagating between two regions with different current densities $\mathbf{j}$, i.e. $\mathbf{j}(x \leq 0) = 0$ and $\mathbf{j}(x > 0) = j_0 \hat{y}$. It is well known that SWs reflect at material boundaries, where the momentum parallel to the interface should be conserved. In the case of SP current, the change in current density is equivalent to an interface, and the momentum perpendicular to ∇j, i.e., $\mathbf{k} \cdot \hat{\tau} \equiv |\mathbf{k} - (\mathbf{k} \cdot \hat{\nabla} j) \hat{\nabla} j|$, with $\hat{\tau}$ the vector tangent to the interface, should be conserved. In our
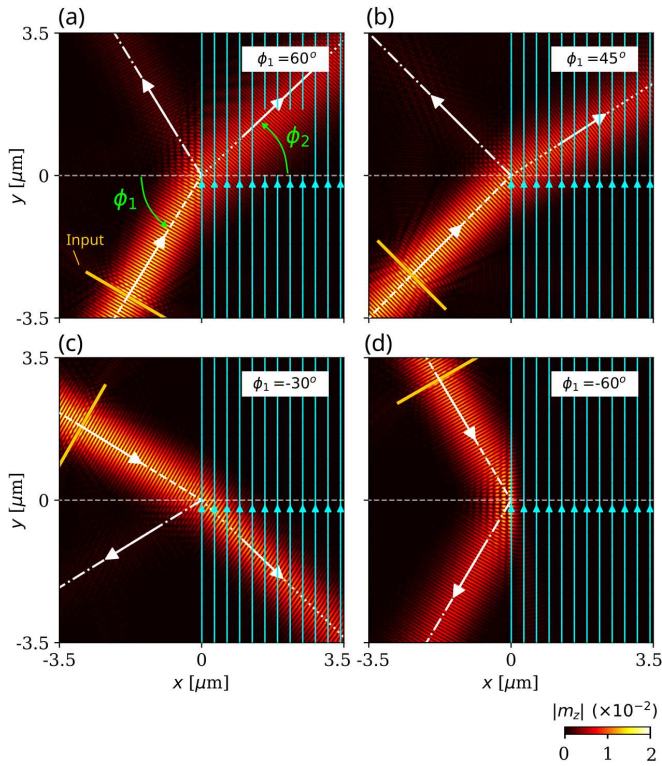
FIG. 2. **Generalized Snell's law for SW refraction**. (a-d) Snapshots of the simulated spin-wave propagation across a sharp interface (at $x = 0$) where the current density changes from 0 to $\mathbf{j} = j_0\hat{y}$, for different incident angles ϕ_1. White arrows indicate the propagation direction following the generalized Snell's law [Eq. (13)]. In these simulations we considered SW frequency $f = 4$ GHz, bias field $H_0 = 0.1$ T applied along $+\hat{x}$ direction, $\mathbf{j} = 2 \times 10^{12}$ Am$^{-2}\hat{y}$, $\alpha = 0.001$ and $\beta = 0.002$. The SW wavelength at zero current is $\lambda \approx 160$ nm.

simple example that corresponds to $k_y^{(1)} = k_y^{(2)}$, where the indices 1 and 2 refer to the incident and refracted waves respectively. If the propagation direction is parallel to the $\mathbf{k}$ vector, the well-known Snell's law applies: $k^{(1)} \sin(\phi_1) = k^{(2)} \sin(\phi_2)$, with ϕ_1 and ϕ_2 the incident and refracted angles respectively. However, since in our case the dispersion relation is asymmetric, the Snell's law has to be adjusted as follows

$$k_g^{(1)} \sin(\phi_1) + \mathbf{k}_0^{(1)} \cdot \hat{\tau} = k_g^{(2)} \sin(\phi_2) + \mathbf{k}_0^{(2)} \cdot \hat{\tau}, \quad (13)$$

where the angles ϕ_i are taken with respect to $\hat{\nabla}j$ (*i.e.*, the direction normal to the interface). Similarly, generalized Snell's laws for the refraction of SWs at domain walls and heterochiral interfaces were derived in Refs. 30 and 22.

To further verify our calculations, we simulate a SW system in the presence of the spin current to calculate the SW refraction when propagating between two regions with different current densities. The SW beams are created by a sinusoidal oscillating field $\mathbf{h} = h_0 \sin(\omega t)\hat{z}$ applied in a narrow rectangular region (input antenna, see Fig. 2 (a)), where the field amplitude h_0 has a Gaussian

profile in the transverse direction and $f = \omega/2\pi$ is the oscillation frequency.

For the simulations, we consider a 20 nm thick magnetic film with saturation magnetization $M_\mathrm{s} = 0.7$ MAm^{-1} and exchange stiffness $A = 10$ pJm^{-1}, corresponding to Permalloy (Ni$_{80}$Fe$_{20}$) thin films, as such films are readily demonstrated as a suitable platform for studying the effects of spin-polarized current on the spin texture[7,18]. In this section, for a better comparison with the analytical results, we assume a low damping constant of $\alpha = 0.001$[31], as we are primarily interested in describing the spin wave propagation direction rather than its amplitude. A more realistic, higher damping constant will be considered in the next section when discussing specific applications. The in-plane bias field is set to $\mathbf{H} = H_0\hat{x}$, with $H_0 = 0.1$ T and we consider $h_0 = 0.01H_0$. The system is discretized into cells of size $10 \times 10 \times 20$ nm^3. The polarization rate of the spin current is set as $P = 0.5$, and the electrical conductivity as $\sigma_0 = 4 \times 10^6$ (Ωm)$^{-1}$.[18] In this section, we neglect AMR effects. Fig. 2 (a-d) shows snapshots of the simulated SW propagation across the interface where the current density sharply changes, for different incident angles ϕ_1. White arrows denote the SW trajectories predicted by our Eq. (13), which are in excellent agreement with the micromagnetic simulations. Notice that the STT induced by the spin current can either deflect or confine the SWs. The critical incident angle ϕ^* above which the SW can not propagate for a given applied current, *i.e.*, the SW undergoes total internal reflection, is obtained from our Snell's law by imposing that the refracted wave is parallel to the interface ($\phi_2 = \pm\pi/2$), as

$$\phi^* = \pm \arcsin\left(\frac{\pm k_g^{(2)} + (\mathbf{k}_0^{(2)} - \mathbf{k}_0^{(1)}) \cdot \hat{\tau}}{k_g^{(1)}}\right). \quad (14)$$

Note that due to the asymmetric dispersion relation, the refraction is not symmetric for positive and negative incident angles. This is seen in the results for $\phi_1 = 60°$ and $\phi_1 = -60°$ in Fig. 2 (a,d), where only for the second case the total reflection of the SW is achieved.

A. Nonuniform current distribution

In practice, the current applied into the magnetic film will not exhibit a step-like distribution as considered in our previous example, but will spread continuously in the material obeying Poisson's equation[32]. To precisely calculate the interaction of SWs with such nonuniform current distributions, we implemented a Poisson solver as described in Sec. II B. Fig. 3 (a) shows a snapshot of the simulated SW propagation across the nonuniform spin current density created between shown finite voltage contacts at the sample edges. Notice that the SW is pertinently deflected while crossing the region where current is applied, to finally reach a shifted propagation direction upon leaving the area pierced by current. Although both the direction and magnitude of the current continuously change as the SW propagates, our general-

ized Snell's law still applies locally - the SW facing a local gradient in current density ∇j is effectively analogous to the earlier interface example. Therefore, the SW trajectory in the presence of a given current distribution $\mathbf{j}(x, y)$ can be solved numerically by iterating the following

$$x^{n+1} = x^n + dr \cos(\phi^{n+1}),$$
$$y^{n+1} = y^n + dr \sin(\phi^{n+1}), \tag{15}$$

where x^n and y^n represent the position coordinates along the trajectory, at the nth iteration; dr is the spatial step size (which here we choose to be the size of a micromagnetic cell), and $\phi^{n+1} = \phi_2(x^n, y^n, \phi^n) + \theta_j^n$ is the propagating angle with respect to the x direction, with θ_j^n the angle between $\hat{\nabla} j|_{x^n, y^n}$ and $+\hat{x}$. Here, ϕ_2 is obtained by applying Eq. (13) locally, between (x^n, y^n) and $(x^n + dr \cos \phi^n, y^n + dr \sin \phi^n)$, with $\phi_1 = \phi^n - \theta_j^n$ the angle of incidence with respect to the local current gradient.

White arrows in Fig. 3 (a) indicate the SW trajectory calculated by iterating Eq. (15) as the SW propagates in the current distribution. The predicted trajectory is in very good agreement with the simulation, demonstrating the general applicability of Eq. (13) even for nonuniform current distributions. Fig. 3 (b) shows the contour plot of the applied current density, where isolines can be seen as interfaces where the SW is refracted. The factor $\Delta k_\perp = (\mathbf{k}_0^{(2)} - \mathbf{k}_0^{(1)}) \cdot \hat{\tau}$ quantifies the change in the propagation direction of the SW and is shown along the SW trajectory as black arrows in Fig. 3 (b). Note that the deflection in trajectory is more pronounced in the regions where the current gradient is sharper.

IV. SELECTED APPLICATIONS

A. Multichannel SW selector

Performing logic operations with SWs generally requires combining different input waves that interfere with each other to generate a desired logic output state[7]. The ability to guide SWs through nanochannels is therefore vital to the development of more complex SW-based circuitry. In this regard, spin currents can be used to precisely guide the SW in such devices, for example, to selectively "write" SWs in one of multiple nanotracks or logic gates in a larger microprocessor. We exemplify here such an application by simulating a multichannel SW selector, illustrated in Fig. 4 (a). In this section, we consider the magnetic parameters for a 20 nm thick $Ni_{80}Fe_{20}$ film, same as in the previous section, but with the damping constant $\alpha = 7 \times 10^{-3}$ stemming from experimental results on Permalloy.[7] The in-plane bias field is set to $H_0 = 0.1$ T, with antenna's excitation field $h_0 = 0.1 H_0$, and the AMR ratio set to 1%.

The input SWs are generated in a channel on the left-hand side of the sample and propagate across a region
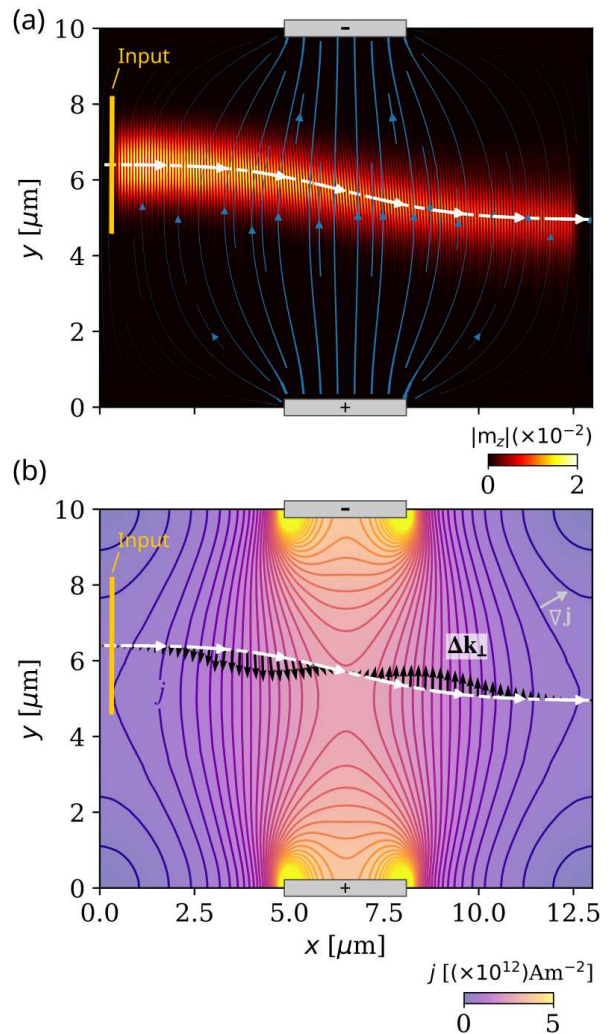
FIG. 3. **SWs under nonuniform current distribution**. (a) Snapshots of the SW propagating across a nonuniform current distribution induced between the voltage contacts (gray regions). White arrows indicate the SW trajectory calculated by iterating Eq. (13) locally along the current gradient in the propagation direction. Parameters are the same as in Fig. 2. (b) Contour plot of the spin current density considered in (a). The shown isolines should be seen as interfaces where the SW is sequentially refracted during propagation. $\Delta \mathbf{k}_\perp$ (black arrows) shows the accompanying change in the propagation direction (see text).

where the spin current is applied. By tuning the magnitude or direction of the applied current one can precisely deflect the SWs towards one of the output channels on the right side of the sample, as shown in Figs. 4 (b, c). Likewise, a frequency selector can be implemented considering the fact that SWs with different frequencies experience different deflections under the same applied current and can therefore be isolated into separate output channels.
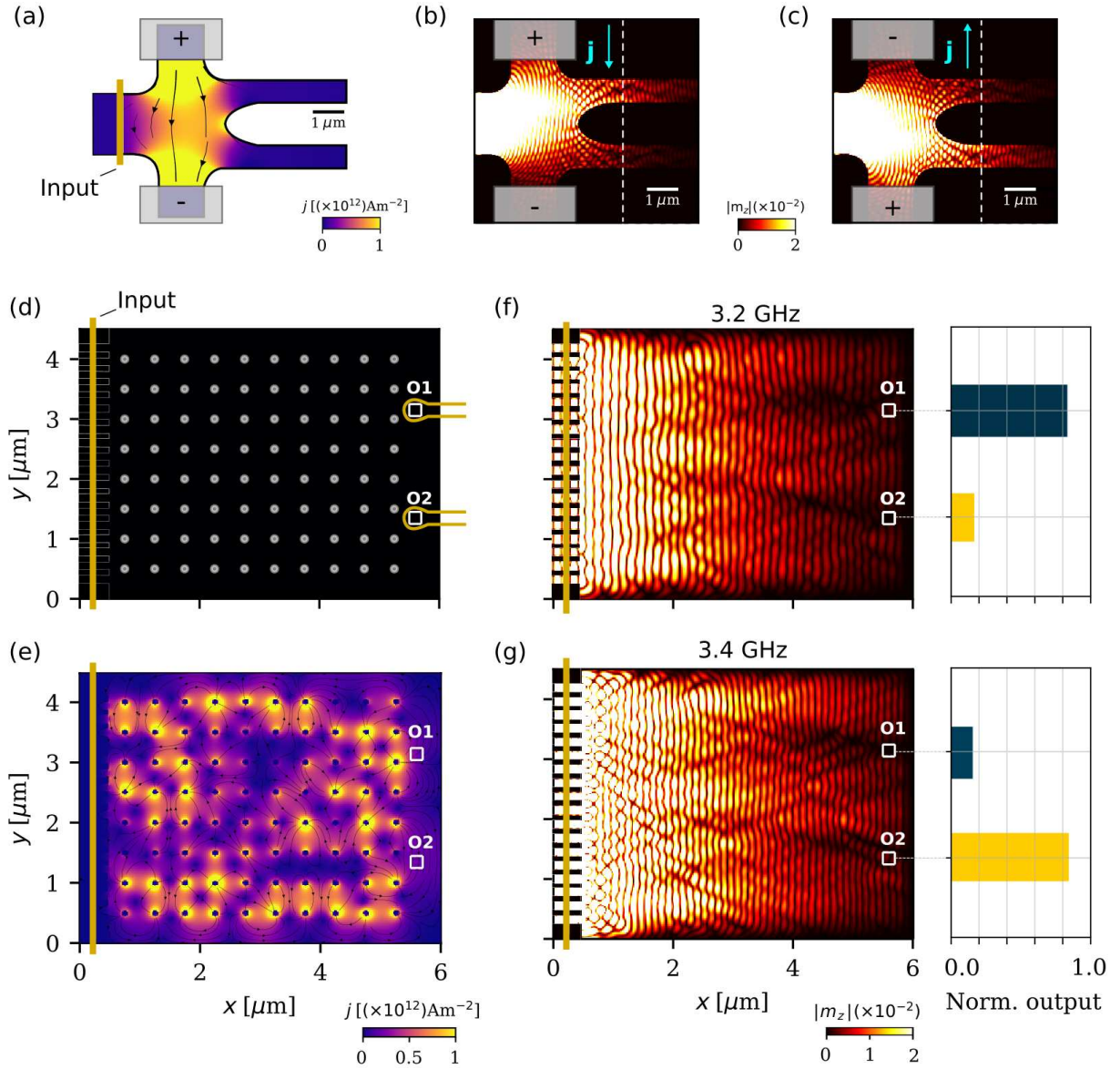
FIG. 4. **Guiding SWs for logic and neuromorphic computing.** (a) A multichannel SW selector demonstrated based on one input and two output channels. Voltage leads induce the spin current in the central region of the sample. (b-c) Snapshots of SW propagation simulated for the setup shown in (a). By changing magnitude or direction of the applied current one can guide the SW towards the desired output channel. (d) Scheme of the envisioned neural network hardware. The (18) input SWs are created on the left and propagate across the matrix of 80 voltage contacts (grey dots) of 100 nm in diameter each. (e) SP-current profile induced by the applied voltage that best performs the desired operation. (f-g) Snapshots of SW simulations after training the neural network. The voltage (current) pattern was trained to focus the waves of two different frequencies to the desired outputs. The bar charts show the normalized intensities at the output locations integrated over 10 ns. In these simulations, we considered SW frequencies $f = 3.2$ GHz (b, c, f) and $f = 3.4$ GHz (g), and magnetic parameters for a 20 nm tick NiFe film (see text).

B. Neuromorphic computing

Finally, we demonstrate the use of SP current for the design of neural-network hardware, based on SW propagation, where weights and interconnections of the network are realized by a pattern of the spin currents applied to the propagating substrate. Fig. 4 (d) illustrates the

envisioned device, where we consider magnetic parameters for a 20 nm tick NiFe film, as reported in the previous section. The input signal is created on the left and propagates across a region with a matrix of 80 voltage contacts (gray dots in Fig. 4 (d)) of 100 nm in diameter each. The read-out is taken from the two output antennas on the right side. An arbitrarily powered voltage matrix induces a distribution of the spin currents in the substrate

	M_s	A	α	P	References
	(MA/m)	(pJ/m)	($\times 10^{-3}$)	$(\Omega m)^{-1}$	
$Ni_{80}Fe_{20}$	0.7	10	7	0.5	[7,18]
CoFeB	1.3	15	4	0.65	[7,33]
CoFeAlB	1.0	9	3		[34]

TABLE I. Material properties of representative low-damping, metallic magnetic materials that can host spin waves and are therefore candidates for the proposed control of SWs by SP current.

that interacts with the input SWs. Training the neural network is equivalent to finding the current pattern that realizes the desired input-output mapping, for example, to classify different input signals by focusing them in different outputs. As suggested in Refs. 4 and 11, a back-propagation machine learning algorithm can be used for training a similar SW-based network, which can perform tasks such as vowel recognition and frequency classification. Here, we demonstrate that a simple Monte Carlo (MC) algorithm can perform the same task of training the neural network for simple classification problems. In our example, we perform a frequency-recognition operation, where we consider input SWs with frequencies $f = 3.2$ and 3.4 GHz. The neural network is trained to focus the SWs with 3.2 GHz to the output O1 and SWs with 3.4 GHz to the output O2 (see Figs. 4 (f, g)). The voltage at each contact is randomly initialized in one of the three values: $U_i = -u_0$, 0 or $+u_0$, with $u_0 = 0.05$ V, and a Metropolis algorithm is implemented by changing the voltage of one of the contacts at every MC step (see supplemental material[28]). The finally trained configuration (resulting in the current distribution shown in Fig. 4 (e)) is able to focus SWs of each frequency to the desired outputs as shown by the bar charts in Figs. 4 (f, g), and can therefore perform the classification operation.

1. Role of material parameters

To identify the role of different material parameters in the current-induced SW scattering, and consequently in the proposed applications, let us consider the case of an SW propagating across two regions with different current densities, as in Fig. 2. In this scenario, for an incident angle $\phi_1 = 0$ and making use of Eqs. (13) and (3), the refraction angle of the SW is given by

$\phi_2 = \sin^{-1}\left(\frac{1+\alpha\beta}{\sqrt{(1+\alpha\beta)^2 + \eta^2}} \right)$, where $\eta = \frac{4e\gamma}{\mu_B} \frac{Ak}{Pj}$. Therefore, the current-induced SW scattering is maximized when η is minimized. In other words, the SW scattering is maximized in materials with small exchange stiffness A and for SWs with small wavenumber k, as well as by increasing the SP current, represented by the polarization P and applied current density j. In Table I we show material properties of representative low-damping, metallic magnetic materials that can host spin waves and

are therefore convenient candidates for the proposed control of SWs by SP current.

2. Effect of Oersted and demagnetizing fields

When nonuniform current is applied into the sample, it inevitably induces an Oersted field. The Oersted field can be calculated from the current density by applying the Biot–Savart law[35]. In our calculations for the neuromorphic application, the resultant Oersted field inside the network presented magnitudes smaller than 1 mT, as shown in Fig. 5 (b) for a single pair of voltage contacts. Such magnetostatic field is much smaller than the considered bias field (100 mT). Therefore, the induced Oersted field is not expected to significantly affect the operation of the considered system. To corroborate that, we calculated the Oersted field from the current distribution in Fig. 4 (e) and verified that the network functionality remains unchanged with Oersted field included, as shown in Fig. 5 (c,d).

On the other hand, the demagnetizing field is generated by the magnetization of the sample. Unlike the Oersted field, the demagnetizing field points in-plane and can shift the SW dispersion relation. Nonetheless, by including the demagnetizing contribution in the training process, one can obtain the current profile that performs the desired classification operation for that scenario. In the supplementary material[28], we show that the proposed network can indeed perform a similar frequency classification in the presence of a demagnetizing field.

One should note that the proposed neuromorphic application can be generalized for arbitrary scenarios, as long as all the relevant magnetic interactions are considered during the training process of the neural network. Moreover, the here proposed fully electronic control enables facilitated reconfiguration and the much-desired scalability of the neural network to perform different tasks within the same integrated circuit.

3. Joule heating and energy dissipation

Another immediate consequence of applying current to the magnetic system is the Joule heating. As the increase of temperature can induce noise and energy dissipation, it might be detrimental for any conceptualized device. Therefore, here we discuss the Joule heating and energy dissipation due to current distribution in our system. The variation of the temperature distribution $T(\mathbf{r}, t)$ in the material as a function of position $\mathbf{r}$ and time t can be obtained by numerically solving the heat equation[36] (see supplementary material[28]). Fig. 5 (e) shows the variation in the temperature distribution obtained in the simulations, for a single pair of voltage contacts, after a five-nanosecond current pulse in the 20 nm thick
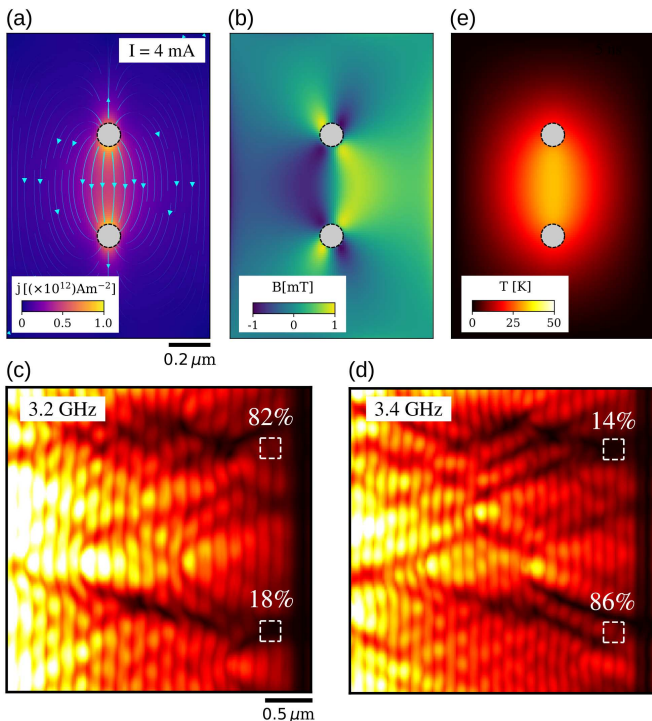
FIG. 5. **Effect of Oersted field and Joule heating on device operation.** (a) Current distribution induced by a single pair of contacts in a 20 nm thick $Ni_{80}Fe_{20}$ thin film, as considered in the neuromorphic application. The total current flowing between the two contacts is set to 4 mA. (b) Oersted field induced by the current density in (a). (c-d) Spin wave intensity (zoomed in near the output contacts) integrated over 10 ns when propagating through the network, with current density as in Fig. 4 (e) and respective Oersted field included, for SW frequencies $f = 3.2$ GHz (c) and $f = 3.4$ GHz (d). Note that the functionality of the network remains unchanged, as indicated by the percentage of the signal that passes through each output (white dashed boxes). (e) Temperature distribution induced by the current density in (a) after a five-nanosecond current pulse, obtained by numerically solving the heat equation for the considered system.

$Ni_{80}Fe_{20}$ film, where we considered the material parameters of Permalloy at room temperature[36]. The regions of highest temperature are located between the contacts, where the current density is highest, while the rest of the sample experiences much smaller thermal effects. In Fig. S2 in the supplementary material[28], we show the maximum temperature variation in the magnetic film as a function of current pulse duration, for different magnitudes of the applied current between the pair of contacts. Note that our calculations do not consider the presence of a substrate, which can reduce the temperature in the magnetic film due to heat dissipation[36].

Since the SWs can propagate with high group velocities, of the order of a micrometer per nanosecond in the $Ni_{80}Fe_{20}$ films[18], and they can be excited at room temperature in such material, the temperature increase during the proposed neuromorphic computations (which takes few nanoseconds to operate) is not expected to invalidate the basic operation of the network. Moreover, the Joule heating can be reduced by decreasing the wavenumber (frequency) of the operating SWs, as explained in what follows.

The power dissipation $\mathcal{P}$ of the isolated pair of electrical contacts is obtained by integrating the Joule heating term $Q = j^2/\sigma_0$ over the sample volume, from where we obtain $\mathcal{P} = 0.01$ to 0.2 mW (pJ/ns) for a range of applied currents from $I = 1$ to 4 mA. The power dissipation of the network is therefore scaled with the number of switched-on contacts. In fact, as discussed previously in this section, the induced deflection in the SW trajectories depends on the ratio between the applied current and the SW wavenumber. Therefore, by reducing the wavenumber of the operating SWs, similar computing operations can be performed with lower applied current, and consequently lower Joule heating and power dissipation, as shown in Fig. S5 in the supplementary material[28]. Hence, for the considered current densities, the proposed device presents similar dissipation as low-power neural networks implemented with both CMOS and beyond-CMOS devices, where energy consumption is of the order of $E = 10^{-11}$ J per operation[11].

V. CONCLUSIONS

We have demonstrated the use of non-uniform spin-polarized current for the manipulation of spin-waves. We showed that the spin-transfer torque induced by the applied current has an effect analogous to DMI for confining spin-waves and controlling their propagation direction in the linear regime, and derived a generalized Snell's law that describes the scattering of spin-waves between regions with different current densities. Finally, we implemented the calculation of the current distribution in micromagnetic simulations by solving the Poisson's equation within the simulation package mumax[3] (to be made available in the upcoming release of mumax[4]), in order to (i) validate the derived Snell's law and (ii) demonstrate how strategically applied current distributions can be employed in magnonic logic and neuromorphic computing devices, thereby advancing the prospects of spintronic hardware and artificial intelligence. Remarkably, our findings underscore the potential for task reprogramming within the same material, thereby offering a level of versatility unattainable with traditional material engineering methods. This progress serves as a significant stride forward in spintronics, hinting at the potential for improvements in the adaptability of spintronic hardware and in the realm of artificial intelligence systems.

* milorad.milosevic@uantwerpen.be

[1] D. V. Christensen, R. Dittmann, B. Linares-Barranco, A. Sebastian, M. Le Gallo, A. Redaelli, S. Slesazeck, T. Mikolajick, S. Spiga, S. Menzel, et al., "2022 roadmap on neuromorphic computing and engineering," Neuromorphic Computing and Engineering (2022).

[2] M. Romera, P. Talatchian, S. Tsunegi, Flavio Abreu A., V. Cros, P. Bortolotti, J. Trastoy, K. Yakushiji, A. Fukushima, H. Kubota, et al., "Vowel recognition with four coupled spin-torque nano-oscillators," Nature 563, 230–234 (2018).

[3] J. M. Shainline, S. M. Buckley, R. P. Mirin, and S. W. Nam, "Superconducting optoelectronic circuits for neuromorphic computing," Physical Review Applied 7, 034013 (2017).

[4] T. W. Hughes, I. A. D. Williamson, M. Minkov, and S. Fan, "Wave physics as an analog recurrent neural network," Science advances 5, eaay6946 (2019).

[5] J. Liu, Q. Wu, X. Sui, Q. Chen, G. Gu, L. Wang, and S. Li, "Research progress in optical neural networks: theory, applications and developments," PhotoniX 2, 1–39 (2021).

[6] H. H. Zhu, J. Zou, H. Zhang, Y. Z. Shi, S. B. Luo, N. Wang, H. Cai, L. X. Wan, B. Wang, X. D. Jiang, et al., "Space-efficient optical computing with an integrated chip diffractive neural network," Nature Communications 13, 1044 (2022).

[7] A. Mahmoud, F. Ciubotaru, A. V. Vanderveken, F.and Chumak, S. Hamdioui, C. Adelmann, and S. Cotofana, "Introduction to spin wave computing," Journal of Applied Physics 128, 161101 (2020).

[8] A. Barman, G. Gubbiotti, S. Ladak, A. O. Adeyeye, M. Krawczyk, J. Gräfe, C. Adelmann, S. Cotofana, A. Naeemi, V. I Vasyuchka, et al., "The 2021 magnonics roadmap," Journal of Physics: Condensed Matter 33, 413001 (2021).

[9] A. V. Chumak, A. A. Serga, and B. Hillebrands, "Magnon transistor for all-magnon data processing," Nature Communications 5, 1–8 (2014).

[10] A. V. Chumak, V. I. Vasyuchka, A. A. Serga, and B. Hillebrands, "Magnon spintronics," Nature Physics 11, 453–461 (2015).

[11] A. Papp, W. Porod, and G. Csaba, "Nanoscale neural network using non-linear spin-wave interference," Nature Communications 12, 1–8 (2021).

[12] S. Zhang and Z. Li, "Roles of Nonequilibrium Conduction Electrons on the Magnetization Dynamics of Ferromagnets," Physical Review Letters 93, 127204 (2004).

[13] D. C. Ralph and M. D. Stiles, "Spin transfer torques," Journal of Magnetism and Magnetic Materials 320, 1190–1216 (2008).

[14] W. Wang, D. Song, W. Wei, P. Nan, S. Zhang, B. Ge, M. Tian, J. Zang, and H. Du, "Electrical manipulation of skyrmions in a chiral magnet," Nature Communications 13, 1–7 (2022).

[15] L. Peng, K. Karube, Y. Taguchi, N. Nagaosa, Y. Tokura, and X. Yu, "Dynamic transition of current-driven single-skyrmion motion in a room-temperature chiral-lattice magnet," Nature Communications 12, 1–7 (2021).

[16] Y. B. Bazaliy, B. A. Jones, and S.-C. Zhang, "Modification of the landau-lifshitz equation in the presence of a spin-polarized current in colossal-and giant-magnetoresistive materials," Physical Review B 57, R3213 (1998).

[17] J. Fernández-Rossier, M. Braun, A. S. Núñez, and A. H. MacDonald, "Influence of a uniform current on collective magnetization dynamics in a ferromagnetic metal," Physical Review B 69, 174412 (2004).

[18] V. Vlaminck and M. Bailleul, "Current-induced spin-wave doppler shift," Science 322, 410–413 (2008).

[19] D. L. Mills and I. E. Dzyaloshinskii, "Influence of electric fields on spin waves in simple ferromagnets: Role of the flexoelectric interaction," Physical Review B 78, 184422 (2008).

[20] J. H. Moon, S. M. Seo, K. J. Lee, K. W. Kim, J. Ryu, H. W. Lee, R. D. McMichael, and M. D. Stiles, "Spin-wave propagation in the presence of interfacial Dzyaloshinskii-Moriya interaction," Physical Review B 88, 184404 (2013).

[21] D. Cortés-Ortuño and P. Landeros, "Influence of the dzyaloshinskii–moriya interaction on the spin-wave spectra of thin films," Journal of Physics: Condensed Matter 25, 156001 (2013).

[22] J. Mulkers, B. Van Waeyenberge, and M. V. Milošević, "Tunable snell's law for spin waves in heterochiral magnetic films," Physical Review B 97, 104422 (2018).

[23] In this paper we use an arrow for 3D vector fields such as the magnetization $\vec{m}$ and the effective magnetic field $\vec{H}_{\text{eff}}$ and bold variables for 2D dimensional vectors in the plane such as the position $\mathbf{r}$, the $\mathbf{k}$-vector, and the current $\mathbf{u}$.

[24] A Thiaville, Y Nakatani, J Miltat, and Yutaro Suzuki, "Micromagnetic understanding of current-driven domain wall motion in patterned nanowires," Europhysics Letters 69, 990 (2005).

[25] A. Vansteenkiste, J. Leliaert, M. Dvornik, M.s Helsen, F. Garcia-Sanchez, and B. Van Waeyenberge, "The design and verification of MuMax3," AIP Advances 4, 107133 (2014).

[26] J. Leliaert, M. Dvornik, J. Mulkers, J. De Clercq, M. V. Milošević, and B. Van Waeyenberge, "Fast micromagnetic simulations on gpu—recent advances made with," Journal of Physics D: Applied Physics 51, 123002 (2018).

[27] D. Prychynenko, M. Sitte, K. Litzius, B. Krüger, G. Bourianoff, M. Kläui, J. Sinova, and K. Everschor-Sitte, "Magnetic skyrmion as a nonlinear resistive element: a potential building block for reservoir computing," Physical Review Applied 9, 014034 (2018).

[28] "See supplemental material at [url will be inserted by publisher] for the calculation of spin-wave dispersion relation under spin-polarized current; monte carlo training of the spin-wave-based neural network; calculation of joule heating, energy dissipation, as well as the effect of demagnetizing field in the proposed spin-wave device," .

[29] S.-M. Seo, K.-J. Lee, H. Yang, and T. Ono, "Current-induced control of spin-wave attenuation," Physical review letters 102, 147202 (2009).

[30] W. Yu, J. Lan, R. Wu, and J. Xiao, "Magnetic Snell's law and spin-wave fiber with Dzyaloshinskii-Moriya interaction," Physical Review B 94, 140410(R) (2016).

[31] A. Papp, W. Porod, A. I. Csurgay, and G. Csaba, "Nanoscale spectrum analyzer based on spin-wave interference," Scientific Reports **7**, 1–9 (2017).

[32] D. J. Griffiths, "Introduction to electrodynamics," (2005).

[33] S. X. Huang, T. Y. Chen, and C. L. Chien, "Spin polarization of amorphous cofeb determined by point-contact andreev reflection," Applied Physics Letters **92**, 242509 (2008).

[34] A. Conca, T. Nakano, T. Meyer, Y. Ando, and B. Hillebrands, "Cofealb alloy with low damping and low magnetization as a candidate for spin transfer torque switching," Journal of Applied Physics **122**, 073902 (2017).

[35] John David Jackson, *Classical electrodynamics* (John Wiley & Sons, 2021).

[36] H. Fangohr, D. S. Chernyshenko, M. Franchin, T. Fischbacher, and G. Meier, "Joule heating in nanowires," Physical Review B **84**, 054437 (2011).